Journal of Materials Chemistry A

RSC Publishing

COMMUNICATION

View Article Online
View Journal | View Issue

Cite this: J. Mater. Chem. A, 2013, 1, 15230

Received 10th September 2013
Accepted 22nd October 2013

DOI: 10.1039/c3ta13624h

www.rsc.org/MaterialsA

Highly dispersed carbon nanotube/polypyrrole core/shell composites with improved electrochemical capacitive performance†

Tao Qian,[a] Xi Zhou,[a] Chenfei Yu,[a] Shishan Wu*[a] and Jian Shen*[ab]

Highly dispersed polypyrrole (PPy) is firstly designed for decorating onto the surface of pristine multiwalled carbon nanotubes (CNTs), then used in the facile synthesis of a CNT/PPy core/shell composite, which provides a potential application for further modification as a base-material due to its high dispersibility. The hybrid material with a PPy shell thickness of 1.61 nm displayed a high specific capacitance of 276.3 F g^{-1} in 1 M KCl electrolyte, four times higher than pristine CNT. Such an improvement in performance is closely correlated with the integrated advantage of the decorated PPy shell, which enhanced the dispersibility and active surface area.

High-energy and power density energy-storage devices are urgently demanded to meet challenges of the ever-increasing development of largescale electric energy storage for renewable energy and sustainable road transport.[1–5] Among the electrochemical energy-storage devices, supercapacitors are considered as one of the promising energy storage devices because of their superior features such as high rate performance, long-term operational stability and friendly environmental impact of composing materials.[6–10] A supercapacitor stores energy through charge accumulation at the electrode/electrolyte interface. Such a charge storage mechanism requires the electrode material to have a sufficiently high surface area and a good electrical conductivity. Nowadays, transition metal oxides,[11,12] carbon materials[13–16] and conducting polymers[17,18] are widely used for electrode materials with prominent capacitive properties.

Carbon nanotubes (CNT) as one of the most widespread carbon materials are an attractive solution for energy storage devices due to their unique properties such as high chemical stability, high aspect ratio, strong mechanical strength, and a relatively high activated surface area.[19,20] In spite of having ideal properties, CNT-based supercapacitors still do not meet the expected performance for capacitance (20–100 F g^{-1}).[21] The specific surface areas of pure CNT film based materials are low because CNT tend to form irreversible agglomerates or even restack, leading to a low capacitance. Much effort has gone into preventing the accumulation of CNT based materials, such as compositing conductive polymers (CP) with CNT.[22–24]

Polypyrrole (PPy) is one of the most promising CP among various CP due to its superior conductivity, electrochemical reversibility, high polarizability, and ease of preparation through chemical or electrochemical routes.[25] Recently, CNT/PPy composite materials have been reported as supercapacitor electrodes for improving the dispersibility with addition of a surfactant and enhancing the performance of capacitance.[26] However, the fabrication process is relatively complex and not easy to control. Herein, in the present work, novel highly dispersed PPy is firstly designed for decoration onto the surface of pristine multiwalled CNTs, which facilely synthesize a CNT/PPy core/shell composite *via* π–π interaction.[27–29] The decorative PPy shell could prevent the aggregation of CNT by electrostatic repulsive interaction between them and lead to a high dispersibility of the prepared composite, which provides a potential application for further modification as a base-material. Moreover, the thickness of the decorated PPy shell is easy to control with the additive amount of the pyrrole–$FeCl_2$–H_2O_2 mixture, which significantly affects the capacitive properties of CNT/CP composite materials (Fig. 1).

To investigate the morphology of the fabricated CNT/PPy core/shell composite with different weight ratios of PPy, scanning electron microscopy (SEM) and transmission electron microscopy (TEM) were carried out and the results are shown in Fig. 2 and 3. The images of pure CNT show a typically smooth surface in Fig. 2A and 3A. By contrast, the surface of nanotubes is rougher after the decoration of PPy, and the diameter increases with the additional amount of PPy particles, which also indicates an increasing thickness of the PPy shell (Fig. 3E

[a]School of Chemistry and Chemical Engineering, Nanjing University, Nanjing 210093, PR China. E-mail: shishanwu@nju.edu.cn; shenj57@nju.edu.cn

[b]College of Chemistry and Materials Science, Nanjing Normal University, Nanjing, 210097, PR China

† Electronic supplementary information (ESI) available: See DOI: 10.1039/c3ta13624h

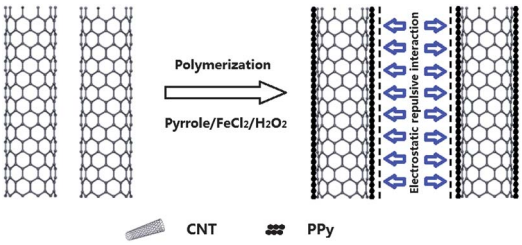

Fig. 1 Scheme showing the chemical route to the synthesis of CNT/PPy core/shell composites.

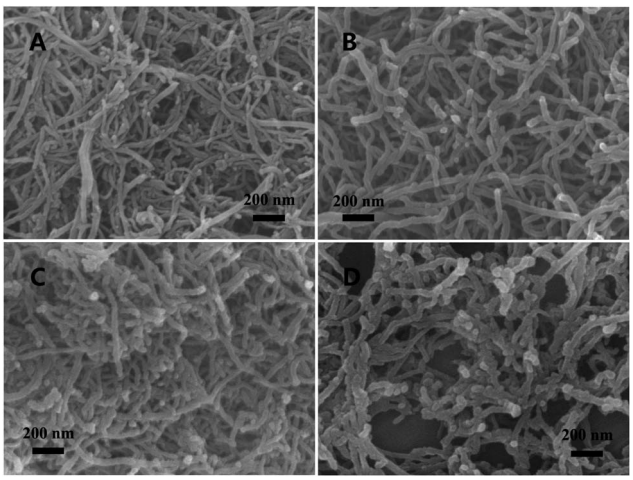

Fig. 2 SEM images of (A) CNT, (B) CNT/$PPy_{0.52}$, (C) CNT/$PPy_{1.61}$, and (D) CNT/$PPy_{3.46}$ composites.

and F). Moreover, it is obvious that there are plentiful PPy nanospheres coated on the core/shell nanotubes due to the excess addition of PPy particles as shown in Fig. 2D and 3D. These phenomena are further confirmed by the transmission electron microscopy (HRTEM) images (see Fig. 3E and F and S1†), and the core/shell structure can be demonstrated clearly with exact scales. The CNT/PPy composites with different average thicknesses of the PPy shell as 0.52, 1.61 and 3.46 nm are named as CNT/$PPy_{0.52}$, CNT/$PPy_{1.61}$, and CNT/$PPy_{3.46}$, respectively (Table S1†).

The structures of the CNT/PPy composites were studied by Raman spectra as shown in Fig. 4. The spectrum of sample CNT contains two strong peaks at 1583 and 1355 cm^{-1} assigned to tangential mode (G-band) and disorder mode (D-band), respectively. The D/G band intensity ratio expresses the atomic ratio of sp^3/sp^2 carbons, which is a measure of the extent of disordered graphite.[30] It is shown that, as the PPy content increases, a significant decrease in the D/G band intensity ratio can be observed. Meanwhile, the characteristic peak for PPy of C–H out-of-plane deformation, ring deformation and C–H in-plane deformation at 925, 981, and 1039 cm^{-1} increases. Both of these phenomena imply the successful fabrication of CNT/PPy hybrids. X-ray photoelectron spectroscopy (XPS) is a powerful technique to discern the surface chemical species of materials. Therefore, the synthesized composites have been

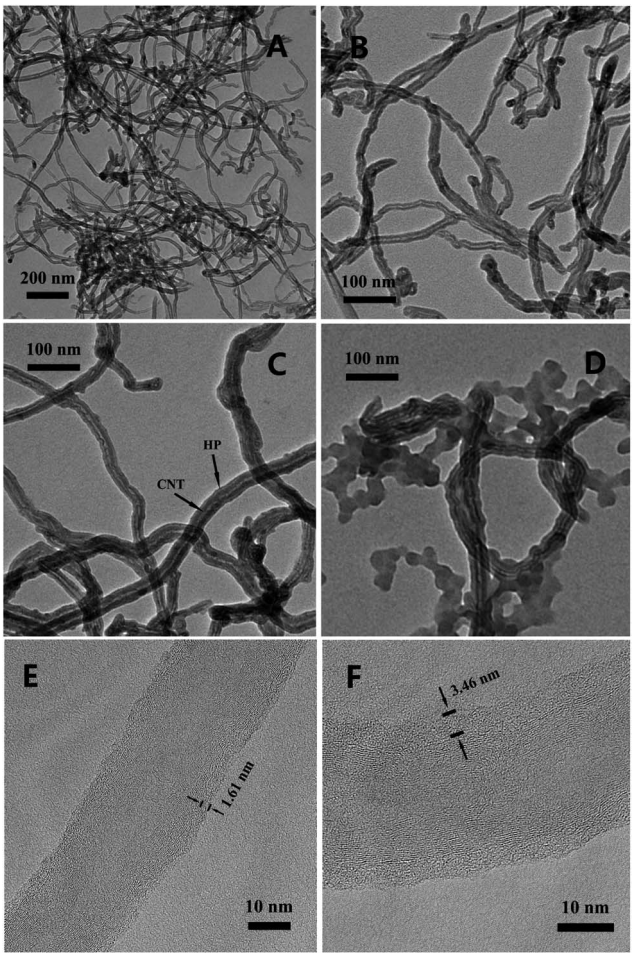

Fig. 3 TEM images of (A) pure CNT, (B) CNT/$PPy_{0.52}$, (C) CNT/$PPy_{1.61}$, (D) CNT/$PPy_{3.46}$, and HRTEM images of (E) CNT/$PPy_{1.61}$, (F) CNT/$PPy_{3.46}$ composites.

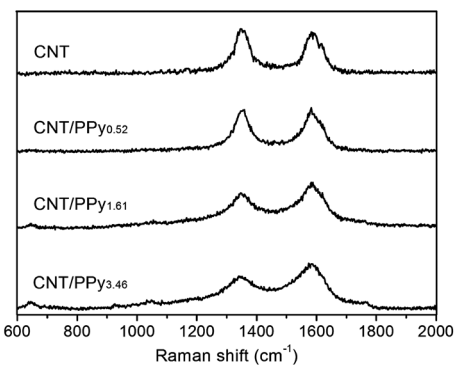

Fig. 4 Raman spectra of pure CNT and CNT/PPy core/shell composites.

subjected to XPS analysis. From careful inspection of wide region spectroscopy (see Fig. S2, ESI†) and elemental analysis of pure CNT and CNT/PPy composites of the XPS study, the peak of N 1s in the CNT/PPy composites was obviously observed, further corroborating the presence of PPy in the concerned composites.

Fig. 5 displays the resulting pictures of the dispersions after sonication to reveal the dispersibility directly perceived through

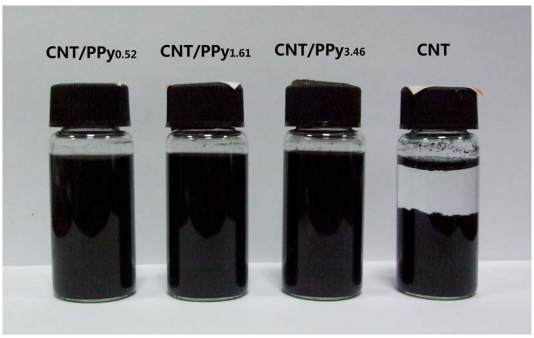

Fig. 5 Photographs of pure CNT and CNT/PPy core/shell composites dispersed in water (1 mg mL^{-1}) after 1 h ultrasonication and a stand for 72 h, pH = 7.0.

naked eye. It can be seen clearly that the CNT dispersion cannot be stably dispersed in aqueous solvents. However, the CNT/PPy composite dispersions exhibit no sedimentation due to the electrostatic repulsive interaction between the decorative PPy shells, which could prevent the aggregation of pristine CNT and lead to a high dispersibility. Table S2, ESI†, presents the data of zeta potentials of pristine CNT and prepared CNT/PPy composites, which are in accordance with the results above.

Cyclic voltammetry (CV) and galvanostatic charge–discharge measurements were employed to evaluate the electrochemical properties and to calculate the specific capacitances of the prepared hybrids. Fig. 6A shows the CV curves of the CNT/PPy$_{1.61}$ electrode at different scan rates. No obvious distortion in the CV curves is observed as the sweep rate increased in the range of 10 mV s^{-1} to 250 mV s^{-1} suggesting a highly reversible system. The galvanostatic charge–discharge curves of the prepared CNT/PPy$_{1.61}$ at different current densities are shown in Fig. 6B, which displays a symmetric shape, indicating a good electrochemical capacitive characteristic. The correlations between specific capacitance (calculated based on the discharge curves) and current densities for various CNT/PPy samples are presented in Fig. 6C. The CNT/PPy$_{1.61}$ has the highest capacity among all samples at the same current density and possess a specific capacitance approaching 276.3 F g^{-1} at 1 A g^{-1}, which is four times higher than that of pure CNT (70.0 F g^{-1}) (see Fig. S5, ESI†). Notably, the capacitance shows only a slight decrease to 220.1 F g^{-1} even at a discharge current density of 10 A g^{-1}, suggesting that the addition of PPy plays a significant role in improving the electrochemical performance of CNT due to the enhancement of effective surface area.

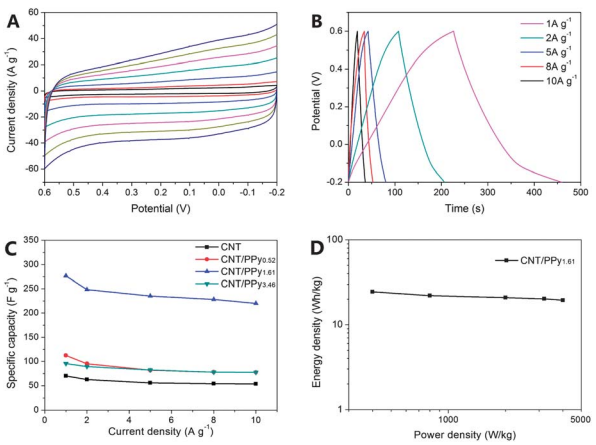

Fig. 6 (A) CVs of the CNT/PPy$_{1.61}$ electrode in 1.0 M KCl solution between −0.2 and 0.6 V at different scan rates; (B) galvanostatic charge–discharge curves of the CNT/PPy$_{1.61}$ supercapacitor with different current densities; (C) the specific capacitances of pure CNT and CNT/PPy core/shell composite modified electrodes at different current densities; and (D) Ragone plots of the CNT/PPy$_{1.61}$ hybrid.

To estimate the effective surface area of the CNT/PPy$_{1.61}$ electrode, CV measurements of these electrodes in a solution containing 10 mM $K_3Fe(CN)_6$ and 0.1 M KCl were performed (see Fig. S3A, ESI†). According to the Randles–Sevcik equation:

$$i_p = (2.687 \times 10^5) n^{3/2} v^{1/2} D^{1/2} A C$$

where i_p refers to the peak current (A) and A is the surface area (cm^2). For 10 mM $K_3Fe(CN)_6$, $n = 1$, $D = 5.7 \times 10^{-6}$ cm^2 s^{-1} (0.1 M KCl), C is the concentration of $K_3Fe(CN)_6$ (M), and v is the scan rate (V s^{-1}). The effective surface area (A) is proportional to $i_p/v^{1/2}$ through this equation.[31,32] The linear relationship between i_p and $v^{1/2}$ is shown in Fig S3B, ESI†. The surface area of a bare GCE is calculated to be 0.067 cm^2, and it compares well with the geometric area of 0.071 cm^2. The calculated effective surface areas of the CNT and CNT/PPy$_{1.61}$ modified electrodes were 0.095 and 0.268 cm^2 respectively. The latter is 2.8 times larger than the former, illustrating that the introduction of a PPy shell effectively enhanced the effective surface area of CNT.

Galvanostatic charge–discharge measurements were carried out at the same current density of 1 A g^{-1} to reveal exactly the electrochemical capacitive performances of different weight ratios as shown in Fig. S4, ESI†. The CNT/PPy composite displays high capacitance due to the enhancement of dispersibility, which originates from the decoration of PPy and leads to a higher surface area. However, the capacitance of CNT/PPy$_{3.46}$ is dramatically reduced compared to that of CNT/PPy$_{1.61}$ because of the poor electrical conductivity of excess conducting polymers. The electrolytic conductivity directly affects the internal resistance of a capacitor which leads to energy loss during charge–discharge cycling.[33,34] The electrolytic conductivity of highly dispersed PPy in the present work is relatively poor due to plenty of oxygenic groups, which lead to a lower specific capacitance (30 F g^{-1} at 1 A g^{-1}) than some other traditional PPy. So this dramatic result could be due to the excessive thickness of the PPy shell and abundant PPy spheres, which play a leading role in the composite. This is further confirmed by the results of UV-vis spectroscopy. Individual CNT are active in the UV-vis region and exhibit characteristic bands,[35] however, bundled CNT are hardly active in the wavelength region between 200 and 600 nm most probably because of carrier tunneling (Fig. 7a).[36] The increasing amount of dispersed CNT results in an increasing effective surface area according to the absorbance of the spectrum. Therefore, UV-vis spectroscopy can be used to monitor the dynamics of this composite process of CNT and PPy, allowing the determination of the optimal weight ratio. The UV-vis spectra of CNT/PPy composite dispersions with different weight ratios show a

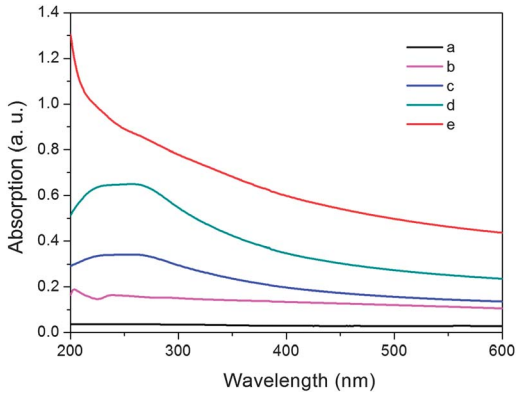

Fig. 7 UV-vis spectra of (a) pure CNT (20 mg L^{-1}), (b) PPy (5 mg L^{-1}), (c) CNT/$PPy_{0.52}$ (25 mg L^{-1}), (d) CNT/$PPy_{1.61}$ (40 mg L^{-1}), and (e) CNT/$PPy_{3.46}$ (100 mg L^{-1}).

maximum between 200 and 300 nm (Fig. 7c and d).[37] However, the characteristic bands of CNT nearly disappear with an excess addition of PPy (Fig. 7e), indicating a lower effective surface area of CNT. This result proves that the excessive thickness of the PPy shell and abundant PPy spheres play leading roles in the composite. All the above phenomena illustrate that the CNT/$PPy_{1.61}$ possesses the optimal capacitive performance mainly owing to its improvement of effective surface area and a suitable thickness of the PPy shell.

Energy and power densities are important factors for evaluating power applications of electrochemical supercapacitors. Fig. 6D shows the Ragone plots of CNT/$PPy_{1.61}$ modified electrodes, which indicate that the CNT/$PPy_{1.61}$ supercapacitors possess a high energy density (24.56 W h kg^{-1}) at a satisfactory power density (0.4 kW kg^{-1}). More importantly, the energy density was very stable with the increase in the power density, and reached up to 19.56 W h kg^{-1} even at a power density as high as 4.00 kW kg^{-1}, much higher than most of the current commercial supercapacitors.

The usable limit of a supercapacitive device depends on its percentage of cycling stability. The cycling stability performance of the CNT/$PPy_{1.61}$ electrode was tested using the galvanostatic charge–discharge technique at a current density of 10.0 A g^{-1}. Fig. 8A reveals the specific capacitance retention as a function of cycle number, which shows a slight decrease at the initial 400 cycles and then remained stable with increasing cycle number. About 86.4% specific capacitance was preserved after 1000 cycles, illustrating a good cycling stability of CNT/$PPy_{1.61}$. The good long-term electrochemical stability of CNT/$PPy_{1.61}$ is further evident from the stable charge–discharge curves for the middle 4 cycles and last 4 cycles (Fig. 8B). The curve shape of the latter is similar to that of the former (497–500 cycles), which remains essentially a symmetric triangular shape.

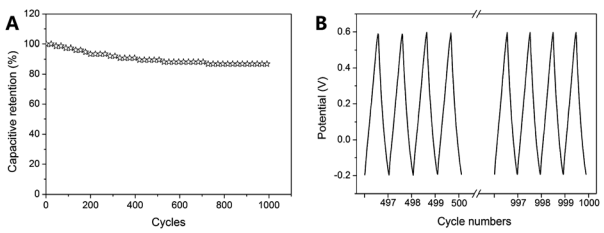

Fig. 8 (A) Cycle stability of CNT/$PPy_{1.61}$ during the long-term charge–discharge process and (B) charge–discharge profile of the CNT/$PPy_{1.61}$ modified electrode for the middle 4 cycles and last 4 cycles at a current density of 10 A g^{-1}.

In conclusion, we report a hybrid core/shell material comprised of CNT and PPy (thickness of the PPy shell is 1.61 nm), which provides a supercapacitor with a specific capacitance of 276.3 F g^{-1} at 1 A g^{-1} and which is capable of delivering an energy density of 24.56 W h kg^{-1} at room temperature. This excellent performance is closely correlated with the integrated advantage of the decoration of the PPy shell with an enhancement of dispersibility and effective surface area. We believe, with such a unique integrated feature, CNT/PPy would also demonstrate a wide potential for further modification as a base-material and application in some other fields such as lithium batteries, fuel cells, and catalysis.

Notes and references

1 B. Kang and G. Ceder, *Nature*, 2009, **458**, 190.
2 H. X. Ji, L. L. Zhang, M. T. Pettes, H. F. Li, S. S. Chen, L. Shi, R. Piner and R. S. Ruoff, *Nano Lett.*, 2012, **12**, 2446.
3 X. L. Wu, L. Y. Jiang, F. F. Cao, Y. G. Guo and L. J. Wan, *Adv. Mater.*, 2009, **21**, 2710.
4 S. W. Lee, N. Yabuuchi, B. M. Gallant, S. Chen, B. S. Kim, P. T. Hammond and Y. Shao-Horn, *Nat. Nanotechnol.*, 2010, **5**, 531.
5 H. Hwang, H. Kim and J. Cho, *Nano Lett.*, 2011, **11**, 4826.
6 P. Simon and Y. Gogotsi, *Nat. Mater.*, 2008, **7**, 845.
7 J. R. Miller and P. Simon, *Science*, 2008, **321**, 651.
8 A. Burke, *Electrochim. Acta*, 2007, **53**, 1083.
9 R. Kotz and M. Carlen, *Electrochim. Acta*, 2000, **45**, 2483.
10 G. H. Yu, X. Xie, L. J. Pan, Z. N. Bao and Y. Cui, *Nano Energy*, 2013, **2**, 213.
11 J. W. Lang, L. B. Kong, W. J. Wu, Y. C. Luo and L. Kang, *Chem. Commun.*, 2008, 4213.
12 C. C. Hu, K. H. Chang, M. C. Lin and Y. T. Wu, *Nano Lett.*, 2006, **6**, 2690.
13 L. M. Li, E. H. Liu, J. Li, Y. J. Yang, H. J. Shen, Z. Z. Huang, X. X. Xiang and W. Li, *J. Power Sources*, 2010, **195**, 1516.
14 M. M. Yang, B. Cheng, H. H. Song and X. H. Chen, *Electrochim. Acta*, 2010, **55**, 7021.
15 C. Z. Wu, X. L. Lu, L. L. Peng, K. Xu, X. Peng, J. L. Huang, G. H. Yu and Y. Xie, *Nat. Commun.*, 2013, **4**, 2431.
16 L. L. Zhang, R. Zhou and X. S. Zhao, *J. Mater. Chem.*, 2010, **20**, 5983.
17 B. K. Kuila, B. Nandan, M. Bohme, A. Janke and M. Stamm, *Chem. Commun.*, 2009, 5749.
18 S. Q. Jiao, J. G. Tu, C. Y. Fan, J. G. Hou and D. J. Fray, *J. Mater. Chem.*, 2011, **21**, 9027.
19 L. Hu, D. S. Hecht and G. Gruner, *Chem. Rev.*, 2010, **110**, 5790.
20 J. Ren, L. Li, C. Chen, X. Chen, Z. Cai, L. Qiu, Y. Wang and H. Peng, *Adv. Mater.*, 2013, **25**, 1155.

21 A. G. Pandolfo and A. F. Hollenkamp, *J. Power Sources*, 2006, **157**, 11.
22 J. Saba, Y. Magga, D. He, F. Miomandre and J. Bai, *Carbon*, 2013, **51**, 20.
23 Z. Cai, L. Li, J. Ren, L. Qiu, H. Lin and H. Peng, *J. Mater. Chem. A*, 2013, **1**, 258.
24 H. Lin, L. Li, J. Ren, Z. Cai, L. Qiu, Z. Yang and H. Peng, *Sci. Rep.*, 2013, **3**, 1353.
25 Z. Zhang, Y. Yuan, L. Liang, Y. Cheng, H. Xu, G. Shi and L. Jin, *Thin Solid Films*, 2008, **516**, 8663.
26 X. Li and I. Zhitomirsky, *J. Power Sources*, 2013, **221**, 49.
27 M. Foroutan and A. T. Nasrabadi, *J. Phys. Chem. B*, 2010, **114**, 5320.
28 X. T. Zhang, Z. Lu, M. T. Wen, H. Liang, J. Zhang and Z. F. Liu, *J. Phys. Chem. B*, 2005, **109**, 1101.
29 Z. Spitalsky, D. Tasis, K. Papagelis and C. Galiotis, *Prog. Polym. Sci.*, 2010, **35**, 357.
30 N. G. Sahoo, Y. C. Jung, H. H. So and J. W. Cho, *Synth. Met.*, 2007, **157**, 374.
31 D. Du, J. Liu, X. Y. Zhang, X. L. Cui and Y. H. Lin, *J. Mater. Chem.*, 2011, **21**, 8032.
32 H. Jiang and X. M. Wang, *Electrochem. Commun.*, 2009, **11**, 126.
33 E. Frackowiak and F. Beguin, *Carbon*, 2001, **39**, 937.
34 K. Zhang, L. L. Zhang, X. S. Zhao and J. S. Wu, *Chem. Mater.*, 2010, **22**, 1392.
35 H. Kataura, Y. Kumazawa, Y. Maniwa, I. Umezu, S. Suzuki, Y. Ohtsuka and Y. Achiba, *Synth. Met.*, 1999, **103**, 2555.
36 J. S. Laurent, C. Voisin, G. Cassabois, C. Delalande, P. Roussignol, O. Jost and L. Capes, *Phys. Rev. Lett.*, 2003, **90**, 057404.
37 N. Grossiord, O. Regev, J. Loos, J. Meuldijk and C. E. Koning, *Anal. Chem.*, 2005, **77**, 5135.

